Regularity and chaos in interacting two-body systems

Sergey Radionov,[1,2,*] Sven Åberg,[1,†] and Thomas Guhr[1,‡]

[1]*Matematisk Fysik, LTH, Lunds Universitet, Lund, Sweden*
[2]*Kiev Institute for Nuclear Research, Kiev, Ukraine*

We study classical and quantum chaos for two interacting particles on the plane. This is the simplest nontrivial case which sheds light on chaos in interacting many-body systems. The system consists of a confining one-body potential, assumed to be a deformed harmonic oscillator, and a two-body interaction of Coulomb type. In general, the dynamics is mixed with regular and chaotic trajectories. The relative roles of the one-body field and the two-body interaction are investigated. Chaos sets in as the strength of the two-body interaction increases. However, the degree of chaoticity strongly depends on the shape of the one-body potential and, for some shapes of the harmonic oscillator, the dynamics remains regular for all values of the two-body interaction. Scaling properties are found for the classical as well as for the quantum mechanical problem.

I. INTRODUCTION

The quantum mechanical correspondence to classical chaos, quantum chaos, is well studied for one-body systems, such as billiard systems, the hydrogen atom in strong magnetic fields, etc.; see, e.g., Refs. [1–5]. In the corresponding quantum system, classical chaos is revealed by the fluctuation properties of energies and wave functions [6]. The connection between classical and quantum chaos is thus, from a practical point of view, rather well understood [7].

Systems consisting of many interacting particles, such as atomic nuclei, quantum dots, and most atoms and molecules, often show spectral fluctuation properties which coincide with those of quantum chaotic systems [8,9]. Although quantum chaos is likely to be the reason for those fluctuation properties in systems with many degrees of freedom, there is no proof for such a conclusion. Moreover, in many-body systems mutual interactions and quantum statistics of particles are expected to play an important role. From this point of view, it is difficult to determine the key mechanism generating irregularity in such systems. If several particles are confined by a one-body field, the dynamics of the one-body field governs the individual motion of the particles. An interesting question is how this is changed if the particles are influenced by a two-body interaction in addition to the one-body field. Can, for example, a system of particles moving in a regular potential show chaotic motion due to the two-body interaction?

To study the combined role of the one-body interaction and the two-body interaction in many-body systems, we shall concentrate on the simplest nontrivial case, namely, the interacting two-body system. Specifically, we consider two identical particles in a two-dimensional deformed harmonic oscillator potential. The motion is regular if the particles are noninteracting. By introducing a two-body interaction between the particles, we may study the role of this interaction in the onset of chaos. The two-body interaction is assumed to be of Coulomb type, where we control the strength of the interaction by a parameter. Also the role of the one-body field may be studied, such as for example, how will the dynamics of the two-body system depend on the shape of the oscillator.

There is a wide literature on studies of chaotic properties of two-body systems [10–12]. In Ref. [13], the origin for the irregularity of quantum spectrum is considered for two particles interacting through short-range potentials. The motion of two charged particles in a billiard is studied in Ref. [14]. Furthermore, there is an attempt to investigate weakly interacting two-body systems in the semiclassical limit by constructing a trace formula [15–17]. In Refs. [18–20], the quantum spectrum is calculated for two-electron anisotropic quantum dots. In these articles a general analysis of the classical phase space and of the fluctuation properties of the energy levels is made at different deformations of the quantum dot. In particular, a peculiarity of the classical dynamics and of the corresponding quantum mechanical spectrum of the system was found at integer frequency ratios of the deformed harmonic oscillator. On the other hand, quantitative descriptions of the classical chaoticity and its dependence on both deformation and excitation energy of the system, scaling properties of the classical and quantum mechanical Hamiltonians have not been considered in these articles. Such questions, in our opinion, are important for the investigation of the appearance of the classical and quantum chaos and will be considered in detail in our paper.

In Sec. II we formulate the general classical problem of motion of many mutually interacting particles confined by a one-body potential. Specifically, we consider two identical charged particles in the field of the two-dimensional deformed harmonic oscillator, interacting via a scaled Coulomb force. By smoothly turning on the strength of the two-body interaction, we can study how chaotic motion sets in for the initially regular dynamics. Using center-of-mass coordinates it becomes possible to consider independently the motion of

*Electronic address: Sergey.Radionov@matfys.lth.se
†Electronic address: Sven.Aberg@matfys.lth.se
‡Electronic address: Thomas.Guhr@matfys.lth.se

the center of mass and relative subsystems. We show how the two-body Hamiltonian can be scaled, thus reducing the number of independent variables in the problem.

Section III is devoted to the quantum mechanical manifestation of the corresponding classical mixed dynamics. In the quantum case we also use the center-of-mass coordinates, leading to a separation of the excitation spectra of the center of mass and relative subsystems. Scaling properties of the quantum mechanical two-body Hamiltonian are also studied. By performing level statistical analysis, we quantify the degree of quantum chaos of the quantum spectrum. The chaoticity of the classical phase space is compared to a fitting parameter characterizing the irregularity of the quantum spectrum (Brody parameter).

Finally, a summary of the main results is given in Sec. IV.

II. CLASSICAL CASE

After setting up the model in Sec. II A, we discuss scaling properties in Sec. II B. The features of the effective potential are investigated in Sec. II C. In Sec. II D, Poincaré surfaces of section are worked out. The dynamics depends on the one-body as well as on the two-body interaction. The influence of the deformation of the confining harmonic oscillator potential is studied in Sec. II E, and that of the scaled energy related to the strength of the two-body interaction in Sec. II F.

A. The model

We consider a system of many identical particles moving in an external confining potential and interacting through two-body central forces. A harmonic oscillator type of confining potential with frequencies ω_x, ω_y, and ω_z can be obtained by expanding the external confining potential around its minimum up to the second order, which is widely used in molecular physics and in the physics of quantum dots.

To gain insight into certain general features of such a system, we consider the simplest nontrivial case, namely, two identical interacting particles on a plane. We notice that the motion of two interacting particles in one dimension is always regular because there are two constants of motion, the total energy in the center of mass and in the relative motion. Only in two or three (or higher) dimensions can the dynamics of the two-body system develop chaos. Such a three-dimensional system can be considered as quasi-two-dimensional under the condition that the oscillatory frequency ω_z of the motion along the z coordinate is much higher than the corresponding frequencies ω_x and ω_y of the motion along the x and y coordinates, $\omega_z \gg \omega_x, \omega_y$, ensuring that the energy of the z motion is negligible compared to the energies of the x and y motions. This is the case, for example, for two interacting electrons confined to a two-dimensional quantum dot.

Hence, the classical Hamiltonian of the system to be studied in the following takes the form

$$\mathcal{H} = \frac{\mathbf{p}_1^2}{2m} + \frac{\mathbf{p}_2^2}{2m} + \frac{1}{2}m(\omega_x^2 x_1^2 + \omega_y^2 y_1^2 + \omega_x^2 x_2^2 + \omega_y^2 y_2^2)$$

$$+ \mathcal{W}(|\mathbf{r}_1 - \mathbf{r}_2|), \qquad (1)$$

where m is the particle mass, $\mathbf{r}_i = (x_i, y_i)$ and $\mathbf{p}_i = (p_{ix}, p_{iy})$, i

$=1, 2$, stand for position and momentum vectors of the particles, and $\mathcal{W}(|\mathbf{r}_1 - \mathbf{r}_2|)$ is the two-body interaction. The corresponding phase space is eight dimensional. Regular dynamics requires the existence of four constants of motion. As the interaction contains a purely distance dependent part, it is natural to introduce center-of-mass coordinates $\mathbf{R} = (\mathbf{r}_1 + \mathbf{r}_2)/2$, $\mathbf{r} = \mathbf{r}_1 - \mathbf{r}_2$, where $\mathbf{R}$ and $\mathbf{r}$ are the center-of-mass and relative vectors, respectively. The Hamiltonian $\mathcal{H}$ now separates, $\mathcal{H} = \mathcal{H}_R + \mathcal{H}_r$, into the center-of-mass Hamiltonian

$$\mathcal{H}_R = \frac{p_X^2}{2M} + \frac{p_Y^2}{2M} + \frac{1}{2}M\omega_x^2 X^2 + \frac{1}{2}M\omega_y^2 Y^2 \qquad (2)$$

and the relative Hamiltonian

$$\mathcal{H}_r = \frac{p_x^2}{2\mu} + \frac{p_y^2}{2\mu} + \frac{1}{2}\mu\omega_x^2 x^2 + \frac{1}{2}\mu\omega_y^2 y^2 + \mathcal{W}(r), \qquad (3)$$

where $M = 2m$ and $\mu = m/2$ are the total and the reduced mass of two identical particles. This advantageous separation is due to the harmonic approximation of the external confining potential. The inclusion of higher than second order terms in expansion of the external potential will, in general, destroy this feature.

The center-of-mass and the relative motion of the system (1) are uncoupled. As can be seen from Eq. (2), the center-of-mass dynamics is regular since the Hamiltonian $\mathcal{H}_R$ is separable with respect to the X and Y axes. Obviously, the energies

$$\mathcal{E}_X = \frac{1}{2}M\omega_x^2 X^2 \quad \text{and} \quad \mathcal{E}_Y = \frac{1}{2}M\omega_y^2 Y^2 \qquad (4)$$

are the two constants of motion for the center-of-mass subsystem.

Thus, we can now focus exclusively on the relative subsystem whose phase space has half of the dimension of the original one. The energy in this subsystem is a constant of motion as well. To see whether or not a second constant of motion exists, we will apply standard tools, in particular, we will work out Poincaré surfaces of section.

Depending on the explicit form of the two-body potential $\mathcal{W}(r)$ in Eq. (3), the dynamics in the relative coordinates can be regular, chaotic, or mixed. Of course, for noninteracting particles $[\mathcal{W}(r) = 0]$ the relative dynamics (3) and, correspondingly, the dynamics of the initial two-body system (1) is regular. The character of the two-particle motion is defined by the form of the mutual two-body interaction. If no harmonic assumption or approximation for the external confining potential is made, chaoticity of the dynamics of interacting two-body systems can also be generated by higher than second order terms, which destroy the separability into center-of-mass and relative motion or by separable, but chaotic center-of-mass dynamics.

B. Scaling properties

To be explicit, we investigate the dynamics of the relative subsystem (3) for two like-charged particles with Coulomb interaction of the form

$$\mathcal{W}(r) = \frac{\alpha}{r}, \tag{5}$$

where the parameter α measures the strength of the two-body interaction. We underline that the ensuing general qualitative study of classical chaos for two identical charged particles (5) applies to any two-body system with a distance dependent force between the particles.

The dynamics is governed by four parameters: the two frequencies ω_x and ω_y of the one-body confining potential, the strength α of the two-body interaction, and the total energy $\mathcal{E}_r$ of the relative subsystem. Luckily, this many-parametric problem greatly simplifies due to scaling properties of the Hamiltonian $\mathcal{H}_r$. The relative dynamics does not depend individually on all four parameters $\omega_x, \omega_y, \alpha, \mathcal{E}_r$, but only on some combination of them. This resembles the situation for the hydrogen atom in a strong magnetic field [5], where the classical dynamics of the electron is determined by a combination of the total energy, E, and the strength parameter of the external magnetic field, γ, as $E/\gamma^{1/3}$.

To find those scaling properties of the relative Hamiltonian (3), we first introduce dimensionless quantities

$$\tilde{\mathbf{r}} = \sqrt{\frac{\mu\omega_0}{\hbar}}\mathbf{r}, \quad \tilde{t} = \omega_0 t, \quad \tilde{\mathcal{H}}_r = \mathcal{H}_r/\hbar\omega_0. \tag{6}$$

Although the present discussion is purely classical, it is convenient for the comparison with the quantum mechanical case later on to use an energy scale involving Planck's constant $\hbar$. We also write

$$\omega_x^2 = \omega_0^2(1 + \varepsilon) \quad \text{and} \quad \omega_y^2 = \omega_0^2(1 - \varepsilon), \tag{7}$$

where the deformation parameter ε measures the deviation from the spherical case which is realized for $\omega_x = \omega_y$. In terms of the frequencies, the deformation parameter is given by

$$\varepsilon = \frac{(\omega_x/\omega_y)^2 - 1}{(\omega_x/\omega_y)^2 + 1}. \tag{8}$$

With these definitions, we obtain the dimensionless Hamiltonian expressed in dimensionless variables,

$$\tilde{\mathcal{H}}_r = \frac{\tilde{\mathbf{p}}^2}{2} + \frac{1}{2}(\tilde{x}^2 + \tilde{y}^2) + \frac{1}{2}\varepsilon(\tilde{x}^2 - \tilde{y}^2) + \frac{\beta}{\sqrt{\tilde{x}^2 + \tilde{y}^2}}. \tag{9}$$

The parameter

$$\beta = \sqrt{\frac{\mu\omega_0}{\hbar}}\frac{\alpha}{\hbar\omega_0} \tag{10}$$

measures the ratio between the strength of the two-body interaction $\mathcal{W}(r)$ and the strength of the one-body confining potential. The original dependence on four parameters is thus reduced to the three parameters scaled energy, ε, and β.

This reduction of parameters can be carried one step further by introducing the coordinates

$$\tilde{\mathbf{r}} = \beta^{1/3}\mathbf{r}_{\text{sc}} \quad \text{and} \quad \tilde{\mathbf{p}} = \beta^{1/3}\mathbf{p}_{\text{sc}}. \tag{11}$$

This yields

$$\tilde{\mathcal{H}}_r(\varepsilon, \beta, \tilde{\mathbf{r}}, \tilde{\mathbf{p}}) = \beta^{2/3}H_{\text{sc}}(\varepsilon, \mathbf{r}_{\text{sc}}, \mathbf{p}_{\text{sc}}) \tag{12}$$

with

$$H_{\text{sc}} = \frac{\mathbf{p}_{\text{sc}}^2}{2} + \frac{1}{2}(x_{\text{sc}}^2 + y_{\text{sc}}^2) + \frac{1}{2}\varepsilon(x_{\text{sc}}^2 - y_{\text{sc}}^2) + \frac{1}{\sqrt{x_{\text{sc}}^2 + y_{\text{sc}}^2}}. \tag{13}$$

Using Eqs. (6) and (12), we find that the energy $\mathcal{E}_r$ of the relative subsystem scales according to

$$E_{\text{sc}} = \beta^{-2/3}\frac{\mathcal{E}_r}{\hbar\omega_0}. \tag{14}$$

Since we will consider only the scaled dynamics of the relative subsystem described by the Hamiltonian H_{sc}, we suppress the index "sc" in the following.

According to the scaled Hamiltonian (13), the dynamics of the relative subsystem depends only on the deformation parameter ε and on the scaled energy $E(\equiv E_{\text{sc}})$; see Eq. (14). Thus the original problem with four parameters is reduced to a problem with two parameters. For a given deformation of the harmonic oscillator the dynamics depends on the scaled energy only. We notice that

$$E = \frac{1}{\mu^{1/3}\omega_0^{2/3}}\frac{\mathcal{E}_r}{\alpha^{2/3}}, \tag{15}$$

as follows from Eqs. (14) and (10).

For the sake of completeness, we mention that the scaling procedure (6)–(14) can be extended to any two-body interaction potential of the form

$$\mathcal{W}(r) = \frac{\alpha}{r^n}. \tag{16}$$

The scaling of the total energy $\mathcal{E}_r$ of the relative subsystem is now given by

$$E = \beta^{-2/(n+2)}\frac{\mathcal{E}_r}{\hbar\omega_0}, \tag{17}$$

where

$$\beta = \left(\frac{\mu\omega_0}{\hbar}\right)^{n/2}\frac{\alpha}{\hbar\omega_0} \tag{18}$$

is the dimensionless parameter.

C. Potential energy landscape

The scaled Hamiltonian H is equivalent to the Hamiltonian for two-dimensional motion of one particle governed by the effective potential

$$V(\mathbf{r}) = \frac{1}{2}(x^2 + y^2) + \frac{1}{2}\varepsilon(x^2 - y^2) + \frac{1}{\sqrt{x^2 + y^2}}. \tag{19}$$

The landscape of the effective potential $V(\mathbf{r}) = V(x, y)$ at fixed deformation parameter $\varepsilon = 0.4$ is shown in Fig. 1(a).

The effective potential is characterized by an infinitely high peak at the origin due to the Coulomb potential
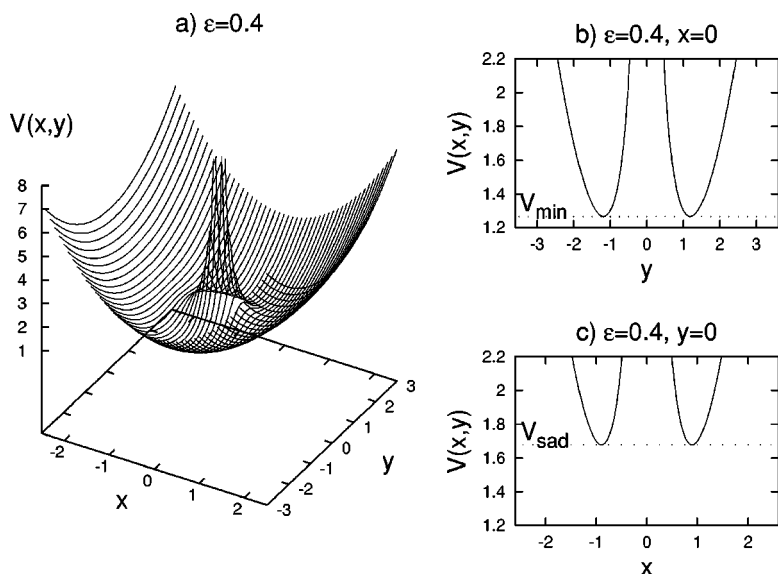
FIG. 1. The landscape of the effective potential (19) at fixed deformation parameter $\varepsilon=0.4$ is displayed in (a). (b) and (c) show the intersections of the surface $V(x,y)$ with the planes $x=0$ and $y=0$.

$1/\sqrt{x^2+y^2}$. For large values of x and y, the potential $V(x,y)$ is dominated by the deformed harmonic oscillator term; see Eq. (19). The details in the structure of the potential energy landscape become clearer when looking at the intersections of the surface $V(x,y)$ with the planes $x=0$ and $y=0$, given in Fig. 1(b) and Fig. 1(c), respectively. The counterplay between the deformed harmonic oscillator and the Coulomb terms in Eq. (19) gives rise to the appearance of two local minima and two saddle points in the potential energy surface.

The positions and corresponding energies of the two local minima shown in Fig. 1(b) are given by

$$y_{\min} = \pm(1-\varepsilon)^{-1/3} \quad \text{and} \quad V_{\min} = \tfrac{3}{2}(1-\varepsilon)^{1/3}, \quad (20)$$

while the positions and energy values of the two saddle points shown in Fig. 1(c) are given by

$$x_{\text{sad}} = \pm(1+\varepsilon)^{-1/3} \quad \text{and} \quad V_{\text{sad}} = \tfrac{3}{2}(1+\varepsilon)^{1/3}. \quad (21)$$

Figure 2 shows the equipotential lines of the effective potential $V(x,y)$.

With increasing energy, the boundary of the equipotential shape becomes more ellipsoidal, and the size of the repulsive center decreases. The motion in such a potential is similar to the one of a particle in an elliptic billiard with a repulsive center.

D. Poincaré surfaces of section

To study the motion governed by the effective potential (19), we use the Poincaré surfaces of section. The dynamical trajectories in the four-dimensional phase space (x,p_x,y,p_y) are obtained numerically from the Hamilton equations of motion. Since the scaled energy E is conserved, we can express the trajectory in a three-dimensional surface by writing p_x as a function of the other variables in Eq. (13),

$$p_x(x,y,p_y) = \pm\sqrt{2E - 2V - p_y^2}. \quad (22)$$

The Poincaré surface of section is then defined as the set of points at which the dynamical trajectories hit the plane
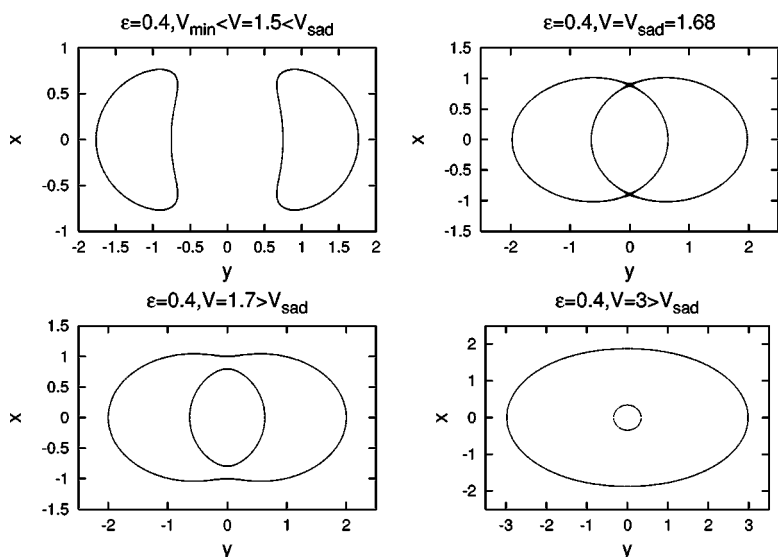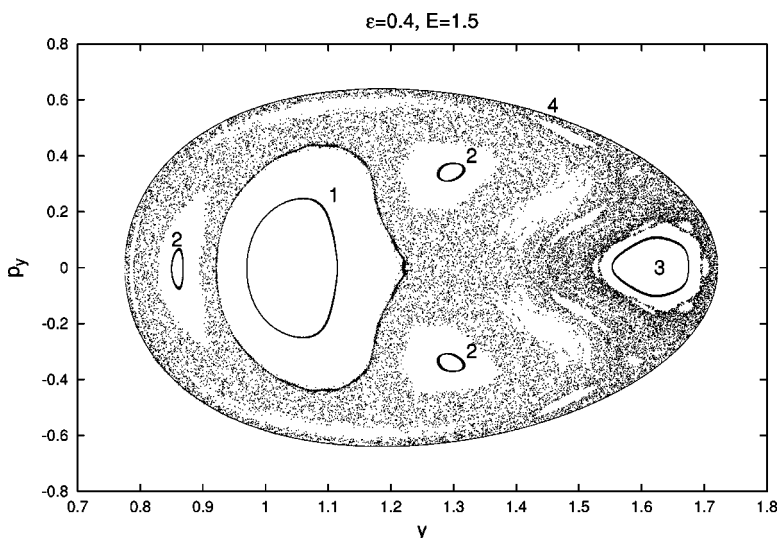

FIG. 2. The equipotential lines of the potential energy surface (19).

FIG. 3. The Poincaré surfaces of section (23) for the scaled energy $E=1.5 < V_{sad}$ at $\varepsilon=0.4$. Dots represent one chaotic orbit. A few regular orbits labeled by digits 1, 2, 3, and 4 correspond to different initial conditions for the Hamilton equations of motion.

$$\Sigma = \{(x,y,p_y)|x=0\}. \tag{23}$$

A Poincaré surface of section for the scaled energy $E=1.5$ at $\varepsilon=0.4$ is depicted in Fig. 3. At this deformation, we have $V_{min}=1.27$ and $V_{sad}=1.68$; see Eqs. (20) and (21). Thus, the energy is below the saddle point energy confining the motion to the sector $y>0$ (or $y<0$) around the minimum; see Fig. 2(a).

A large part of the phase space is filled by one chaotic trajectory shown by the gray area in Fig. 3. The dynamics is mixed, and the different white areas correspond to regular trajectories, of which we show four examples in Fig. 3 denoted as 1, 2, 3, and 4. Orbit 1 surrounds the elliptic fix point that corresponds to a bouncing ball motion in the y direction close to $y=1$. Orbit 4 is the pure one-dimensional motion along the y axis at $x=0$ and $p_x=0$ that defines the border of the allowed phase space in Fig. 3. The fixed point close to orbit 3 corresponds to a banana-shaped orbit in the x-y plane bouncing from $x \approx 0.4, y \approx 0.7$ to $x \approx -0.4, y \approx 0.7$; see Fig. 2(a). Orbit 2 is a more complicated three-periodic orbit. A

hierarchy of complicated regular orbits fill the white areas in Fig. 3 and give rise to a fractal structure of the phase space.

In Fig. 4, we show Poincaré surfaces of section for two scaled energies above the saddle point energy, $E=3$ [Fig. 4(a)] and $E=10$ [Fig. 4(b)]. At both energies, one chaotic orbit covers most parts of the available phase space. In Fig. 4(b) we also show one regular six-periodic orbit.

In contrast to the previous case, the particle has enough energy to pass the saddle point, and moves in both of the regions $y>0$ and $y<0$. This is reflected in the presence of two ovals in the Poincaré surfaces of section. As expected, by increasing the scaled energy E, the relative fraction of chaotic motion decreases. This feature is due to general properties of the Hamiltonian E. Larger energies E correspond either to larger absolute values of x and y, or to higher momenta p_x and p_y. In the first case, the contribution from the Coulomb potential in Eq. (19) becomes smaller compared with the contribution from the deformed harmonic oscillator. Therefore, the dynamics becomes more regular. In the second case, higher velocities imply that the dynamics of the
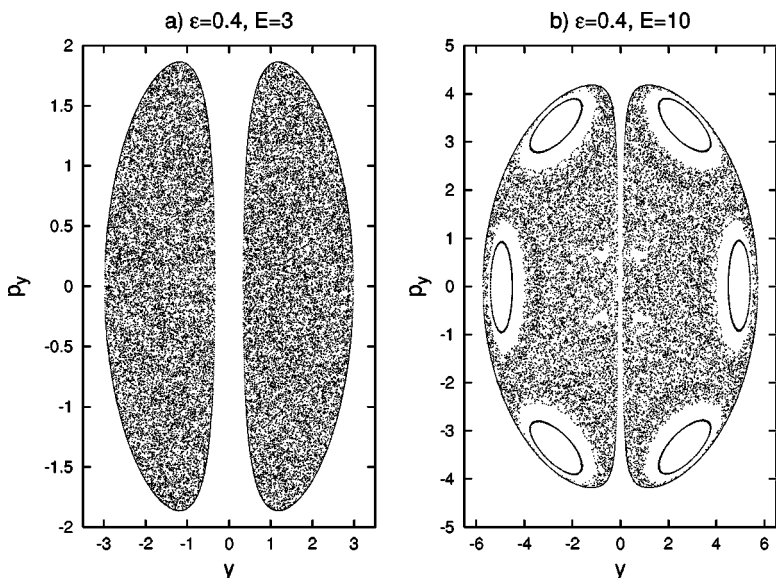

FIG. 4. The examples of the Poincaré surfaces of section (23) for the scaled energies $E=3$ and $E=10$ above the saddle point energy (21) at deformation $\varepsilon=0.4$. As the energy E increases, the fraction of chaotic parts of phase space decreases.
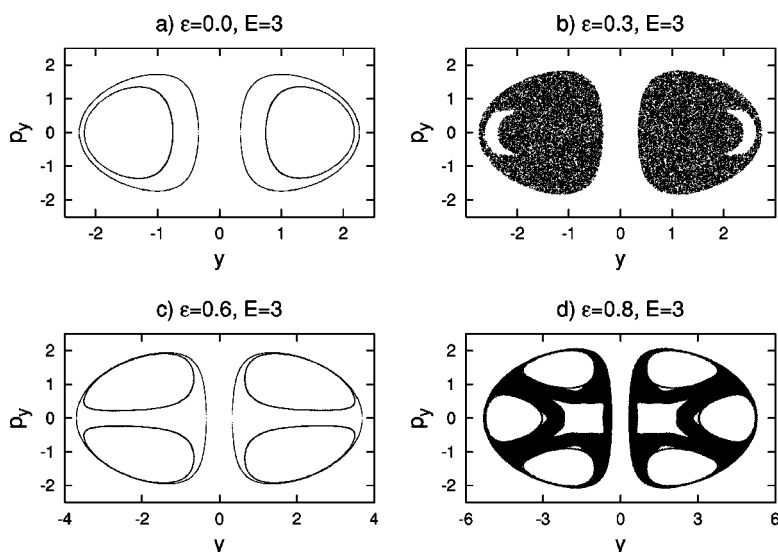
FIG. 5. The dependence of the Poincaré surfaces of section (23) on the deformation parameter ε [Eq. (8)] at fixed scaled energy $E=3$. We notice that $E=3$ is above the saddle point energy (21) for every $\varepsilon \in [0,1]$. In the cases $\varepsilon=0$ (1:1 deformation), and $\varepsilon=0.6$ (2:1 deformation), the classical phase space is regular due to the presence of second constants of motion, the square of the angular momentum and Eq. (24), respectively. For the deformation parameter $\varepsilon=0.8$ corresponding to the integer frequency ratio $\omega_x/\omega_y = 3$ (3:1 deformation), the classical phase space is mostly regular due to the degeneracy of the effective potential (19) for integer ω_x/ω_y.

system is less sensitive to the structure of the effective potential (19); see Fig. 1.

E. Dependence of the chaoticity on the deformation

To investigate the effect of the one-body potential on the chaoticity, we study the dependence of chaotic trajectories in the phase space (13) on the deformation parameter ε.

By definition (8), ε measures the ratio between the x and y axes of the ellipsoidal equipotential shapes of the potential energy surface (19); see Fig. 2. For example, shapes with 1:1, 2:1, and 3:1 ratios are obtained for $\varepsilon=0$, 0.6, and 0.8, respectively. For $\varepsilon=0$, i.e., $\omega_x/\omega_y=1$, the dynamics of the relative subsystem (13) is regular because we have spherical symmetry. The square of the angular momentum is the second constant of motion. Remarkably, a second constant of motion also exists at the deformation $\varepsilon=0.6$, i.e., for the 2:1 shape of the oscillator, $\omega_x/\omega_y=2$. This constant of motion is related to the Runge-Lenz vector and was analytically constructed in Ref. [22]. In our notation it reads

$$I = yp_xp_y - xp_y^2 + y^2x - \frac{x}{\sqrt{x^2+y^2}}. \tag{24}$$

Thus, the important question arises whether integrability is restricted to these two deformations, or if a second constant of motion exists at other deformations as well. Since the motion is regular at 1:1 and 2:1 deformations, the 3:1 deformation is the first natural case to look for regular motion. To illustrate the dependence of the dynamics (13) on the deformation parameter ε, we work out the Poincaré surfaces of section for four values of ε at fixed scaled energy $E=3$, as shown in Fig. 5. This value of the scaled energy is above the saddle point energy (21) for every $\varepsilon \in [0,1]$.

It is reassuring for our numerics that it reveals a completely regular phase space for $\varepsilon=0$ and $\varepsilon=0.6$, i.e., for 1:1 and 2:1 ratios of the x and y axes. The 3:1 deformation corresponds to $\varepsilon=0.8$, and the Poincaré surface of section is shown in Fig. 5(d). Is there a second constant of motion in this case or not?—as the phase space is mostly regular, one is, at first sight, tempted to expect the presence of a second

constant of motion. However, there is indeed chaotic motion in a part of the phase space, excluding a second constant of motion at this deformation parameter. By constructing the Poincaré surfaces of section for the 4:1, 5:1, 6:1, etc., ratios, we find that the degeneracy of the Hamiltonian H arising at integer frequency ratios ω_x/ω_y leads to the relatively large regularity of the phase space, but chaotic regions exist for all studied deformations.

It therefore seems unlikely that a second constant of motion exists for shapes other than 1:1 and 2:1. Thus, we conclude from our numerics that the phase space comprises a mixture of chaotic and regular orbits for all deformations, except 1:1 and 2:1. To characterize the classical dynamics, we numerically calculate the relative weight of chaotic regions in the totally available phase space (13). We introduce a chaoticity parameter q which measures the ratio between the area covered by chaotic trajectories and the total area of allowed phase space in the Poincaré surface of section. The two limits $q=0$ and $q=1$ correspond to completely regular and chaotic dynamics, respectively.

In Fig. 6, the chaoticity parameter $q=q(E,\varepsilon)$ of the classical phase space is displayed as a function of the deformation parameter ε at fixed scaled energy $E=3$.

At $\varepsilon=0$ and $\varepsilon=0.6$ the motion of the system (13) is completely regular such that $q=0$ for all scaled energies. The remarkable feature becoming clear from Fig. 6 is the nonmonotonic dependence of $q=q(E,\varepsilon)$ on the deformation parameter ε. Distinct local minima are present at the integer frequency ratios $\omega_x/\omega_y=3$, 4, 5, and 6. A similar result was found in Ref. [18].

An infinite set of local minima of the function $q = q(E,\varepsilon)$ seems to appear for all integer ratios $\omega_x/\omega_y = \ldots, 7, 8, 9, \ldots$. In the limit $\varepsilon \to 1$, the relative fraction of chaoticity of the classical phase space can be estimated to $q \to 0.52$. The limit $\varepsilon \to 1$ is reached for $\omega_x \gg \omega_y$ [see Eq. (8)], which corresponds to quasi-one-dimensional motion along the y axis. On the other hand, putting $\varepsilon=1$ in the Hamiltonian (13) leads to Hamiltonian equations for unbounded motion along the y axis, which is completely regular, since any one-dimensional motion is regular. The dynam-
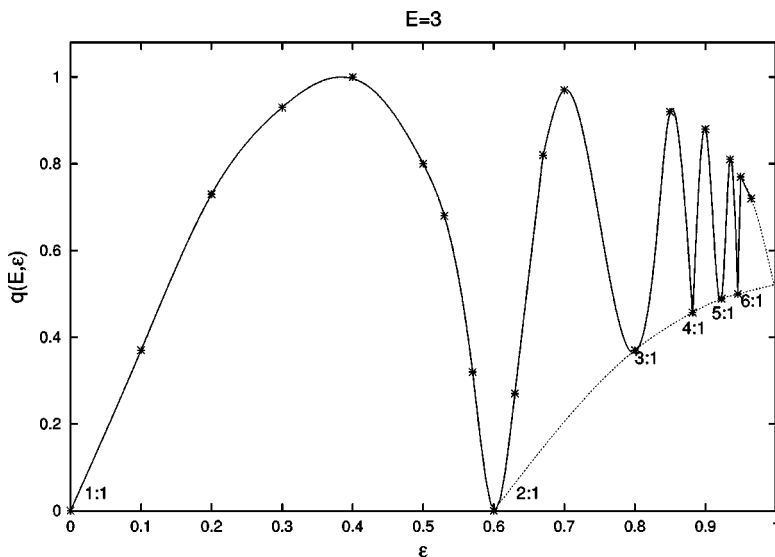
FIG. 6. The dependence of the chaoticity parameter $q=q(E,\varepsilon)$ on the deformation parameter ε at the scaled energy $E=3>V_{\text{sad}}(\varepsilon)$. Local minima at 0.8, 0.88, 0.92, and 0.97 correspond to the integer frequency ratios $\omega_x/\omega_y=3$, 4, 5, and 6, respectively. In the limit $\varepsilon\rightarrow 1$, the chaoticity parameter q approaches the value 0.52. The stars mark the numerically calculated values of q; the solid line is a spline interpolation to guide the eye.

ics in the quasi-one-dimensional case is thus quite different from the dynamics in one dimension. In a similar way non-integrability is introduced by accounting for the third dimension in a quasi-two-dimensional system [21].

Another interesting feature visible in Fig. 6 is the behavior of the parameter q near the global minimum at $\varepsilon=0.6$. We have checked that $q=q(E,\varepsilon)$ in this region is a smooth function of the deformation parameter ε. Thus, the Kolmogoroff-Arnold-Moser theorem [1] can be used to study the transition from regularity to chaos at this value of the deformation parameter. Of course, this also applies to the more trivial case of $\varepsilon=0$.

F. Dependence of the chaoticity on the scaled energy

Investigating the dependence of chaotic motion on the scaled energy $E\sim\mathcal{E}_r/\alpha^{2/3}$ requires us to simultaneously study the role of the relative energy in the two-body system, $\mathcal{E}_r$, and the dependence on the strength α of the two-body interaction.

In Fig. 7 we show how the degree of chaoticity depends on the scaled energy E at the two deformations $\varepsilon=0.4$ (left-hand figure) and $\varepsilon=0.55$ (right-hand figure). The q values are numerically calculated at energies marked in the figure.

An important structure of the dynamics governed by the Hamiltonian H is borne out in Fig. 7: Below the saddle point energy (marked by an arrow) most orbits are regular. The corresponding motion is restricted to the area around one local minimum; see Fig. 2(a). As the energy is increased to values above the saddle point, the particle can move in the entire plane, and an ever larger fraction of chaotic orbits appears. The chaotic dynamics has a distinct maximum for an energy just above the saddle point energy V_{sad}. When the energy is increased even more, the effect due the Coulomb interaction in Eq. (19) becomes less important, and the area of regular orbits increases. We notice that the scaled energy becomes larger either with growing total energy $\mathcal{E}_r$ of the relative subsystem or with decreasing strength α of the Coulomb interaction; see Eq. (15).

For a fixed value of the total energy, changes in the scaled energy are due to varying strength α of the two-body interaction. The noninteracting case then corresponds to $\alpha\rightarrow 0$,
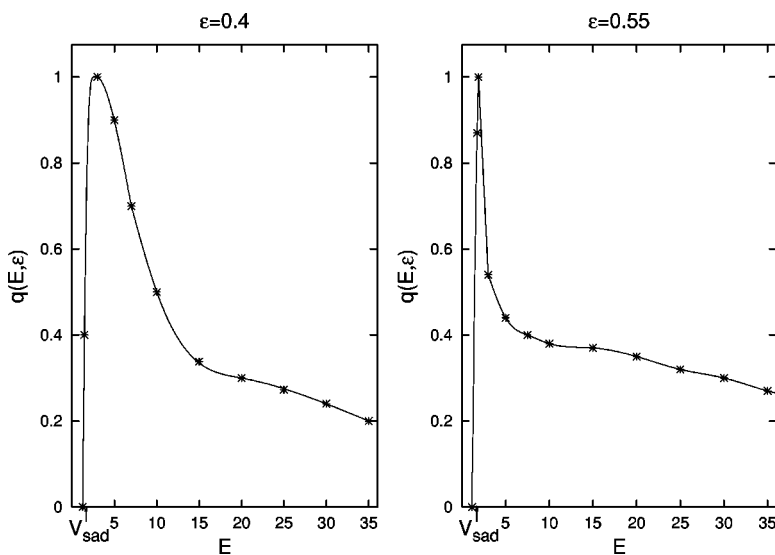

FIG. 7. The ratio $q=q(E,\varepsilon)$ between the area of chaotic regions and the total area of allowed phase space in the Poincaré surfaces of section (23) versus the scaled energy E at fixed deformation parameter $\varepsilon=0.4$ (left) and $\varepsilon=0.55$ (right). A similar dependence on E is expected for every deformation parameter ε. With increasing energy E, the relative fraction q of chaotic orbits decreases. The stars mark the numerically calculated values of q the solid line is a spline interpolation to guide the eye.

i.e., $E \rightarrow \infty$. In this limit the motion of the two noninteracting particles is regular at all deformations, as already seen in Eq. (1). The onset of the two-body interaction is prompted by a decreasing value of the scaled energy. Figure 7 shows how chaos smoothly sets in with increasing strength of the two-body interaction at both deformations. At the special deformations $\varepsilon = 0$ and $\varepsilon = 0.6$, the motion is regular for all values of the scaled energy. In those cases the onset of the strength of the two-body interaction has no impact on the dynamics which remains regular.

III. QUANTUM MECHANICAL CASE

We now address the quantum mechanical manifestation of classical chaos for our system. In Sec. III A, we set up the Hamilton operator and draw certain conclusions for the quantum statistics. After discussing scaling properties in Sec. III B, we sketch the numerical computation of the spectra in Sec. III C. We investigate the spectral statistics in Sec. III D.

A. Hamilton operator and quantum statistics

The Hamilton operator $\hat{H}$ corresponding to the classical system (1) in the center-of-mass coordinates decouples analogously to the classical case, $\hat{\mathcal{H}} = \hat{\mathcal{H}}_R + \hat{\mathcal{H}}_r$, where the center-of-mass $\hat{\mathcal{H}}_R$ and the relative $\hat{\mathcal{H}}_r$ Hamilton operators are quantized versions of the corresponding classical Hamiltonians (2) and (3). Thus, the wave function of the total two-body system can be written as the product $\Theta(\mathbf{r}_1, \mathbf{r}_2) = \Theta_R(\mathbf{R})\Theta_r(\mathbf{r})$ of the wave functions Θ_R and Θ_r for the center-of-mass and the relative subsystems, respectively. The total energy is the sum $\mathcal{E}_{qm} = \mathcal{E}_{qm,R} + \mathcal{E}_{qm,r}$ where the center-of-mass energy $\mathcal{E}_{qm,R}$ and the relative energy $\mathcal{E}_{qm,r}$ are found from

$$\hat{\mathcal{H}}_R \Theta_R(\mathbf{R}) = \mathcal{E}_{qm,R} \Theta_R(\mathbf{R}),$$

$$\hat{\mathcal{H}}_r \Theta_r(\mathbf{r}) = \mathcal{E}_{qm,r} \Theta_r(\mathbf{r}). \tag{25}$$

Obviously, we have

$$\mathcal{E}_{qm,R} = \left(K_x + \tfrac{1}{2}\right)\hbar\omega_x + \left(K_y + \tfrac{1}{2}\right)\hbar\omega_y \tag{26}$$

for the center-of-mass energy with two good quantum numbers K_x and K_y. We eliminate this integrable part from our consideration, and concentrate on the study of the energy spectrum $\mathcal{E}_{qm,r}$ of the relative subsystem in Eq. (25) at fixed quantum numbers K_x, K_y.

So far, we have not taken the spins $\mathbf{s}_1$ and $\mathbf{s}_2$ of the particles into account. However, this has to be done to understand the quantum statistics of our problem. As there is no coupling between the orbital and the spin motions, we can write the total wave function in the form

$$\Psi(\mathbf{r}_1, \mathbf{s}_1; \mathbf{r}_2, \mathbf{s}_2) = \Theta_R(\mathbf{R})\Theta_r(\mathbf{r})\Phi(\mathbf{s}_1, \mathbf{s}_2), \tag{27}$$

where $\Phi(\mathbf{s}_1, \mathbf{s}_2)$ is the spin wave function. To discuss the quantum statistics of the two interacting particles, we distinguish bosons and fermions. First, for two bosons, $\Psi(\mathbf{r}_1, \mathbf{s}_1; \mathbf{r}_2, \mathbf{s}_2)$ should be symmetric under interchange of

the particles 1 and 2 ($\mathbf{r}_1 \leftrightarrow \mathbf{r}_2, \mathbf{s}_1 \leftrightarrow \mathbf{s}_2$). Since in this case the center-of-mass function $\Theta_R(\mathbf{R})$ and the spin wave function $\Phi(\mathbf{s}_1, \mathbf{s}_2)$ are always symmetric under the interchange of two particles, the relative function $\Theta_r(\mathbf{r})$ must be also symmetric, i.e., have positive parity, $\Theta_r(-\mathbf{r}) = \Theta_r(\mathbf{r})$. Second, in the case of two interacting fermions the total wave function $\Psi(\mathbf{r}_1, \mathbf{s}_1; \mathbf{r}_2, \mathbf{s}_2)$ must be antisymmetric, which means that if the spin function $\Phi(\mathbf{s}_1, \mathbf{s}_2)$ is symmetric the relative function $\Theta_r(\mathbf{r})$ must be antisymmetric, i.e., have negative parity, $\Theta_r(-\mathbf{r}) = -\Theta_r(\mathbf{r})$.

The parity of the relative function $\Theta_r(\mathbf{r})$ defines the symmetry properties of the total wave function function $\Psi(\mathbf{r}_1, \mathbf{s}_1; \mathbf{r}_2, \mathbf{s}_2)$. As we will see below, for the Coulomb interaction (or any other purely distance dependent interaction) the eigenstates of the relative subsystem separate into solutions with negative and positive parity, respectively.

A comment on possible experimental study of the energy spectrum for the two-body interacting system $\hat{\mathcal{H}}$ is in order. Mostly, one measures the electric dipole radiation of the system. The intensity is proportional to the square of the center-of-mass vector $\mathbf{R}$. As the quadratic confining potential for the center-of-mass subsystem does not affect the relative dynamics, the excitation spectrum of the total two-body system $\hat{\mathcal{H}}$ is defined only by the excitation of the center-of-mass subsystem. This is true for every two-body interaction between the particles. Hence, one cannot measure the energy spectrum of the relative subsystem by electric dipole transitions. Only by measuring transitions with higher multipolarities, information about the influence of the mutual interaction between particles on the two-body energy spectrum can be extracted; see Refs. [23,24].

B. Scaling properties

Before calculating the quantum mechanical energies $\mathcal{E}_{qm,r}$, we compare the scaling properties of the classical Hamiltonian $\mathcal{H}_r$ (3) for the relative subsystem with the corresponding quantum mechanical Hamiltonian operator $\hat{\mathcal{H}}_r$. Using Eqs. (6) and (11), we rewrite the Schrödinger equation in the same dimensionless variables that we introduced in the classical case. We have

$$\hat{H}\Theta_r(x,y) = E_{qm}\Theta_r(x,y), \tag{28}$$

where $\Theta_r(\mathbf{r}) = \Theta_r(x,y)$ and

$$\hat{H} = -\frac{1}{2}\frac{\partial^2}{\partial \mathbf{r}^2} + \frac{1}{2}(x^2 + y^2) + \frac{1}{2}\epsilon(x^2 - y^2) + \frac{\beta}{\sqrt{x^2 + y^2}}. \tag{29}$$

The scaled energy reads

$$E_{qm} = \frac{\mathcal{E}_{qm,r}}{\hbar\omega_0}. \tag{30}$$

The parameter β is given by Eq. (10). In contrast to the classical Hamiltonian (3), the Hamilton operator $\hat{H}$ does not scale with the parameter β. However, by exploiting Eqs. (14) and (13), we can formally achieve one-to-one correspondence with the classical scaled Hamiltonian H by putting β

=1. The fixing of the parameter β implies that we fix the number of energy states involved in consideration. Because of the practical limitation on the size of the matrix consisting from the matrix elements of $\hat{H}$, we cannot consider the semiclassical limit $\hbar \rightarrow 0 (\beta \rightarrow \infty)$, when the correspondence between classical and quantum mechanical cases should hold.

C. Computation of the spectra

To obtain the eigenvalues E_{qm} of the Hamilton operator (29), we numerically diagonalize the problem (28). As basis wave function, we choose the eigenfunctions of the deformed harmonic oscillator, $\langle x,y|n_x,n_y\rangle$, that is, the exact eigenfunctions of $\hat{H}$ in the absence of the Coulomb interaction, characterized by the good quantum numbers n_x and n_y. With these basis functions, we compute the matrix elements $\langle n_x,n_y|\hat{H}|n'_x,n'_y\rangle$.

This choice of basis wave functions implies the following selection rules for the matrix elements of the Coulomb interaction:

$$\left\langle n_x,n_y \left| \frac{1}{\sqrt{x^2+y^2}} \right| n'_x,n'_y \right\rangle \neq 0 \quad \text{if} \quad (-1)^{(n_x+n_y)}=(-1)^{(n'_x+n'_y)},$$

$$\left\langle n_x,n_y \left| \frac{1}{\sqrt{x^2+y^2}} \right| n'_x,n'_y \right\rangle = 0 \quad \text{if} \quad (-1)^{(n_x+n_y)} \neq (-1)^{(n'_x+n'_y)}.$$

$$(31)$$

This is so because the Coulomb potential is an even function of the x and y variables, implying that the matrix element vanishes if the Hermitian polynomials yield an even or odd function in the integrand. Thus, a parity $\gamma=(-1)^{(n_x+n_y)}$ can be assigned and the (truncated) matrix with matrix elements $\langle n_x,n_y|\hat{H}|n'_x,n'_y\rangle$ is block diagonal in γ. According to Eq. (31), γ defines the spatial parity $(x \rightarrow -x, \ y \rightarrow -y)$ of the relative function $\Theta_r(\mathbf{r})=\Theta_r(x,y)$.

As discussed above, parity has a different impact for two-fermion or two-boson systems. We will consider positive and negative parity separately, but later on we will add the information from both spectra when studying statistical properties.

There are additional constants of motion at the 1:1 and 2:1 shapes in classical mechanics. Correspondingly, an additional quantum number exists at each of these two deformations in the quantum case. The Hamilton operator $\hat{H}$ commutes with the square angular momentum operator in the circular case (1:1), and with the operator

$$\hat{I} = y\frac{\partial^2}{\partial x \, \partial y} - x\frac{\partial^2}{\partial y^2} + y^2x - \frac{x}{\sqrt{x^2+y^2}}, \quad (32)$$

at the 2:1 deformation. However, these additional symmetries are not exploited in the calculation of the spectra. This gives us an extra check of our numerical procedures at the 1:1 and 2:1 shapes (see Fig. 11 below).

In solving the Schrödinger equation (28) numerically, we use truncated matrices of the size 555×555, constructed from the matrix elements $\langle n_x,n_y|\hat{H}|n'_x,n'_y\rangle$. This is done sepa-

rately for positive and negative parity, $\gamma=+1$ and $\gamma=-1$, respectively. The limited sizes of the matrices leads to numerical errors in the calculation. To estimate the number of calculated eigenvalues which can be used with sufficiently high precision, we compared the results of the computations carried out with truncated matrices of different sizes. By comparing the energy eigenvalues from calculations with 355×355 and 555×555 matrices we find that the lowest 72% of the eigenvalues are calculated with an error less than 0.1%. In the calculations presented below we have used the first 400 energy levels from the totally 555 calculated eigenvalues.

D. Spectral statistics

For systems with two degrees of freedom the relation between classical and quantum mechanics has been investigated in a large number of cases. The studies confirm the Bohigas-Giannoni-Schmit conjecture [2–4,6]. It states that the quantum system should show spectral fluctuations of the Wigner-Dyson type if the corresponding classical system is fully chaotic while other spectral fluctuation, often of the Poisson type, are expected if the corresponding classical system is regular. In these cases, the distributions $p(s)$ of spacings s between adjacent levels are given by

$$p(s) = \frac{\pi}{2}s \exp\left(-\frac{\pi}{4}s^2\right) \quad \text{and} \quad p(s) = \exp(-s) \quad (33)$$

for Wigner-Dyson and Poisson statistics, respectively. Recently, progress has been made in proving this conjecture [25,26]. Thus, in our case, we expect that the spectra of the quantized relative motion show these limits as well.

A more difficult situation arises for mixed classical dynamics, since its quantum manifestation is a highly nontrivial issue. In a rather general form, this is studied in terms of the Bohigas-Tomsovic-Ullmo model [27] which can be viewed as an extension of the Bohigas-Giannoni-Schmit conjecture. Due to the complexity of the classical phase space, no simple and generic form for the nearest neighbor spacing distribution can be conjectured. Nevertheless, one often uses the purely phenomenological Brody distribution [28]

$$p(s) = (q+1)\sigma_q s^q \exp(-\sigma_q s^{q+1}),$$

$$\sigma_q = \Gamma^{q+1}\left(\frac{q+2}{q+1}\right), \quad (34)$$

where $\Gamma(x)$ is the Γ function. For $q=0$ and $q=1$, the Brody distribution becomes the Poisson or the Wigner-Dyson distribution, respectively. For values $0<q<1$ of the parameter q, the Brody distribution interpolates between the Poisson and the Wigner-Dyson distribution. Importantly, one has $p(0)=0$ at $s=0$ for all $q>0$. This is tantamount to having no disconnected regions in phase space.

To measure the spectral fluctuations independently of the level density, one proceeds as follows [2–4,29]. In Fig. 8, the counting function $N(E_{qm})$ is shown for the first 50 positive parity energy levels calculated at two deformation parameters $\varepsilon=0.4$ and $\varepsilon=0.55$. The counting function $N(E_{qm})$ gives
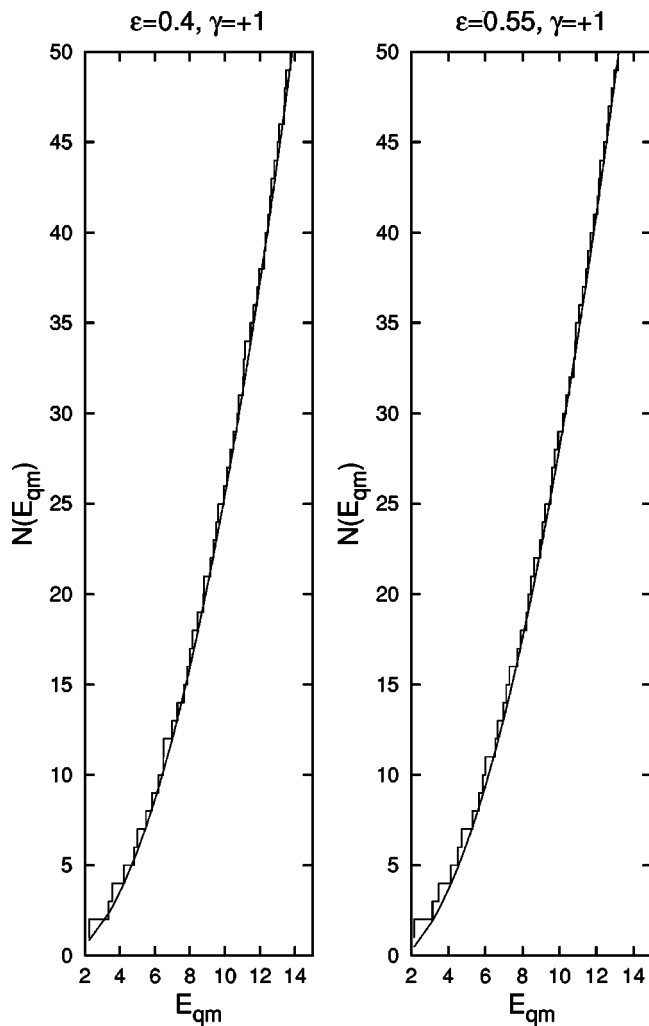
FIG. 8. Counting function $N(E_{qm})$ for the first 50 levels with positive parity $\gamma = +1$, on the left hand side for deformation parameter $\varepsilon = 0.4$, on the right hand side for deformation parameter $\varepsilon = 0.55$. The solid lines are the corresponding smooth parts of the counting function, obtained by fitting a second order polynomial.

the number of energy states less than or equal to E_{qm}. One decomposes the counting function into a smooth part $\widetilde{N}(E_{qm})$ and a fluctuating part $N_{fl}(E_{qm})$, such that $N(E_{qm}) = \widetilde{N}(E_{qm}) + N_{fl}(E_{qm})$. The derivative of the smooth part is the level density $\rho(E_{qm}) = d\widetilde{N}(E_{qm})/dE_{qm}$. We fit this smooth part of the counting function, i.e., the cumulative level density, with a quadratic polynomial. The fit by quadratic polynomials is done separately for the positive and negative parity spectra. The fit is very good; examples are shown in Fig. 8.

The level density is unfolded from the spectra by mapping the energies $E_{qm,n}$ onto new energy variables $\xi_n = \widetilde{N}(E_{qm,n})$, $n = 1, 2, 3, \ldots$. The spacings between adjacent levels are the differences $s_n = \xi_{n+1} - \xi_n$, $n = 1, 2, 3, \ldots$.

For the comparison between empirical or numerical data with formulas such as Eqs. (33) and (34), one often employs the cumulative spacing distributions

$$F(s) = \int_0^s p(s')ds', \tag{35}$$

which is the probability to find spacings smaller than or equal to s. Advantageously, $F(s)$ is in contrast to $p(s)$ independent of binning effects.

In Fig. 9 we show the cumulative spacing distribution for two values of the deformation parameter $\varepsilon = 0.4$ and $\varepsilon = 0.55$ obtained from the numerical calculation. Both positive-parity and negative-parity states are included in the distribution function. Fitting the cumulative spacing distribution with the help of Eqs. (34) and (35), we get $q \approx 0.9$ for $\varepsilon = 0.4$ and $q \approx 0.4$ for $\varepsilon = 0.55$.

The resulting nearest neighbor spacing distributions $p(s)$ for these two cases at $\varepsilon = 0.4$ and $\varepsilon = 0.55$ are depicted in Fig. 10.

We find that the nearest neighbor spacing distribution is almost fully compatible with the Wigner-Dyson case for the spectrum at $\varepsilon = 0.4$ and that it is between Wigner-Dyson and Poisson at $\varepsilon = 0.55$. We conclude that our statistical analysis
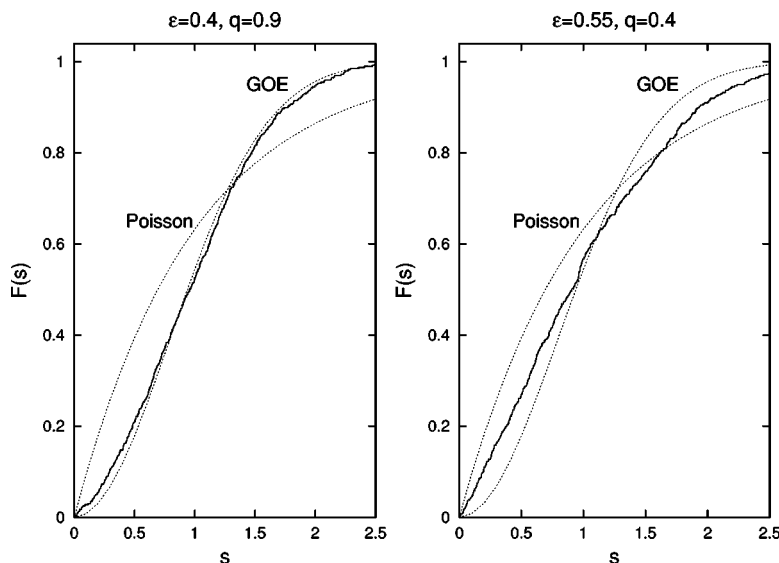

FIG. 9. The cumulative spacing distribution $F(s)$ calculated for the deformation parameters $\varepsilon = 0.4$ and $\varepsilon = 0.55$. The fit gives $q \approx 0.9$ for $\varepsilon = 0.4$ and $q \approx 0.4$ for $\varepsilon = 0.55$. For comparison, the cumulative Poisson and Wigner-Dyson statistics are also shown as dotted lines.
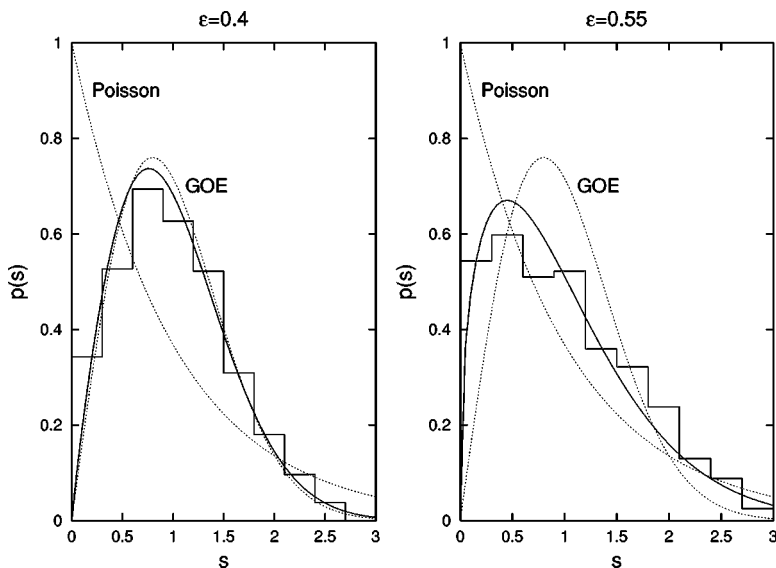
FIG. 10. The nearest neighbor spacing distribution $p(s)$ for two values of deformation parameter $\varepsilon=0.4$ and $\varepsilon=0.55$, obtained from the numerics (histograms). The lowest calculated 400 positive-parity and negative-parity energy states are included. The solid lines show the Brody distributions resulting from the fit of the cumulative spacing distributions. For comparison, the Poisson and the Wigner-Dyson spacing distributions are also shown as dotted lines.

is consistent with the expectation from the Bohigas-Giannoni-Schmit conjecture.

We also constructed the nearest neighbor spacing distribution $p(s)$ for two special deformation parameters $\varepsilon=0.0$ and $\varepsilon=0.6$ for which the Hamiltonian $\hat{H}$ commutes with the square angular momentum operator and with the operator (32), respectively. Results are presented in Fig. 11. We see high peaks at small spacings s which can be explained by the shell structure of the energy levels at both deformation parameters ε. Despite the fact that at these deformations the classical system is regular, the nearest neighbor spacing distribution $p(s)$ does not follow the Poisson statistics as can be expected from the Bohigas-Giannoni-Schmit conjecture. The deviation is originating from the high degeneracies of the energy levels at these two shapes of the confining potential, and the deviations from Poisson statistics is similar to what is well known for the deformed harmonic oscillator potential.

We want to settle with this qualitative observation. A more quantitative comparison between the classical and the quantum mechanical results would be very difficult, because

it would require a much more detailed prediction for the spacing distribution. Here, we stress once more that the Brody distribution is purely phenomenological. It is encouraging that it yields a satisfactory description of the numerical data, but we would find it questionable to more deeply interpret the mixing parameter q obtained from the fit. Moreover, the limited energy window of the quantum mechanical calculation also severely limits the possibility for quantitative comparison between classical and quantum mechanical cases.

IV. SUMMARY

In an attempt to achieve some deeper understanding of how chaos emerges in interacting many-body systems, we investigated the simplest nontrivial many-body system. We studied two particles in two dimensions subject to a confining one-body field and to a two-body interaction. The system has four degrees of freedom, and is in general quite complicated. In order to simplify, we assumed the one-body field to
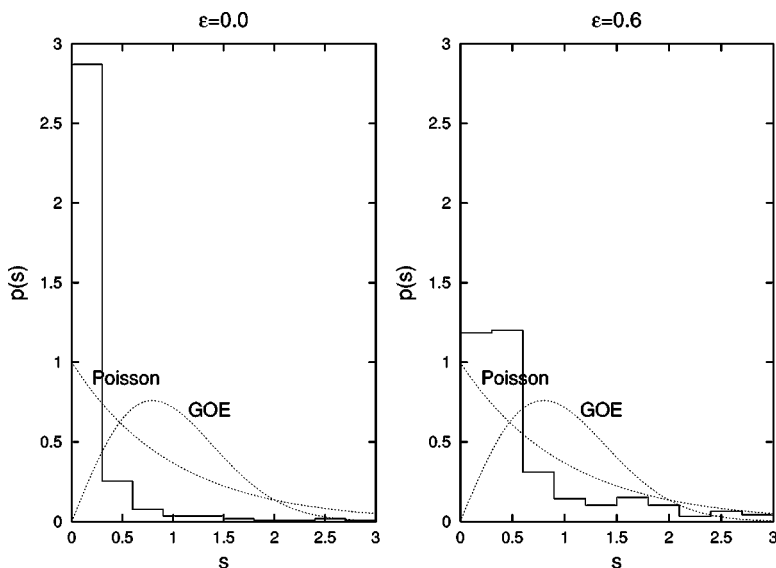

FIG. 11. Spacing distribution $p(s)$ for the deformation parameters $\varepsilon=0$ and $\varepsilon=0.6$ both corresponding to classically regular motion.

be a deformed harmonic oscillator, and the two-body interaction to be a Coulomb interaction α/r, where we treated the strength α as a parameter. Due to the harmonic character of the confining potential, only the relative subsystem can give rise to chaotic motion, while the center-of-mass dynamics is always regular. We employed center-of-mass coordinates to reduce the total four-dimensional dynamics of the interacting two-body system to the two-dimensional dynamics of the relative subsystem.

The relative dynamics is defined by the frequencies ω_x and ω_y of the deformed harmonic oscillator, by the strength α of two-body interaction, and by the total energy $\mathcal{E}_r$ of the relative subsystem. We have shown that for the Coulomb interaction (or for any other purely distance dependent interaction) the relative Hamiltonian $\mathcal{H}_r$ can be scaled [see Eqs. (3)–(13)]. The scaling dynamics (13) depends only on the scaled energy E (14) and on the deformation parameter ε (8), which measures the relation between the frequencies ω_x and ω_y. The scaling of the energy implies that the dynamics does not depend independently on the (relative) energy $\mathcal{E}_r$ and on the strength α of the two-body force, but on the combined relation $E \sim \mathcal{E}_r/\alpha^{2/3}$.

The classical phase space of the relative subsystem shows a rich structure with mixed dynamics of regular and chaotic trajectories. The dynamics was studied by numerically solving the classical Hamiltonian equations of motion, and by the construction of Poincaré surfaces of section. The fraction of chaotic orbits in the allowed phase space, q, was studied for different values of the two independent parameters, deformation and scaled energy.

The degree of chaoticity was found to increase as the strength of the two-body interaction was increased (or as the relative energy decreased). However, the explicit shape of the one-body field (deformed harmonic oscillator) was found to play a most important role. In particular, since the motion in the circular $(1:1)$ and in the $2:1$ shapes is integrable, the dynamics is always regular, independent of the strength of the two-body interaction. We also found local minima of the degree of chaoticity [as measured by the parameter q $=q(E,\varepsilon)$] at deformations of the harmonic oscillator corresponding to integer values of ω_x/ω_y; cf. Refs. [18,19].

For small values of the scaled energy the motion was found to be near regular for all shapes. The motion is then confined around one of the two local minima in the potential energy surface of the relative motion coordinates. As the scaled energy is increased to values close to the saddle point in the potential energy, the size of the chaotic phase space takes a maximum. The size of the chaotic phase smoothly decreases as the scaled energy increases. For very large values of the scaled energy, corresponding to very small values of the strength of the two-body interaction, the motion approaches regularity.

The corresponding quantum mechanical problem was also investigated. The excitation of the center-of-mass subsystem could be characterized by two good quantum numbers which are the quantum numbers of the deformed harmonic oscillator operator. Therefore, quantum chaos for the interacting two-body system could appear only due to dynamics of the relative subsystem.

To estimate statistical fluctuations in the energy spectrum of the relative subsystem we solved numerically the corresponding Schrödinger equation. After unfolding the energy spectrum, the nearest neighbor spacing distribution, and the corresponding cumulative distribution, were studied.

Very recently, we became aware of the very recent work of Ref. [19] that already contains some of the results which we also obtained in the quantum mechanical case.

[1] M. C. Gutzwiller, *Chaos in Classical and Quantum Mechanics* (Springer, New York, 1990).

[2] H.-J. Stöckmann, *Quantum Chaos: An Introduction* (Cambridge University Press, Cambridge, England, 1999).

[3] F. Haake, *Quantum Signatures of Chaos*, 2nd ed. (Springer, Berlin, 2001).

[4] T. Guhr, A. Müller-Groeling, and H. A. Weidenmüller, Phys. Rep. **299**, 189 (1998).

[5] H. Friedrich and D. Wintgen, Phys. Rep. **183**, 37 (1989).

[6] O. Bohigas, M. J. Giannoni, and C. Schmit, Phys. Rev. Lett. **52**, 1 (1984).

[7] M. Berry, Eur. J. Phys. **2**, 91 (1981).

[8] O. Bohigas, R. U. Haq, and A. Pandey, in *Nuclear Data for Science and Technology*, edited by K. H. Böchhoff (Reidel, Dordrecht, 1983), p. 809.

[9] N. Rosenzweig and C. E. Porter, Phys. Rev. **120**, 1698 (1960).

[10] K. Patel, M. S. Desai, V. Potbhare, and V. K. B. Kota, Phys. Lett. A **275**, 329 (2000).

[11] L. Kaplan and T. Papenbrock, Phys. Rev. Lett. **84**, 4553 (2000).

[12] F. Borgonovi, I. Guarneri, F. M. Izrailev, and G. Casati, Phys. Lett. A **247**, 140 (1998).

[13] M. Van Vessen, M. C. Santos, B. K. Cheng, and M. G. E. da Luz, Phys. Rev. E **64**, 026201 (2001).

[14] L. Meza-Montes and S. E. Ulloa, Phys. Rev. E **55**, R6319 (1997).

[15] J. Sakhr and N. D. Whelan, Phys. Rev. A **62**, 042109 (2000).

[16] D. Wintgen, K. Richter, and G. Tanner, Chaos **2**, 823 (1992).

[17] D. Wintgen, A. Burgers, K. Richter, and G. Tanner, Prog. Theor. Phys. Suppl. **116**, 121 (1994).

[18] P. S. Drouvelis, P. Schmelcher, and F. K. Diakonos, Europhys. Lett. **64**, 232 (2003).

[19] P. S. Drouvelis, P. Schmelcher, and F. K. Diakonos, Phys. Rev. B **69**, 035333 (2004).

[20] P. S. Drouvelis, P. Schmelcher, and F. K. Diakonos, J. Phys.: Condens. Matter **16**, 3633 (2004).

[21] R. G. Nazmitdinov, N. S. Simonovic, and J. M. Rost, Phys. Rev. B **65**, 155307 (2002).

[22] G. Baumann and T. F. Nonnenmacher, Phys. Rev. A **46**, 2682 (1992).

[23] P. A. Maksym, Physica B **249**, 233 (1998).

[24] F. M. Peeters, Phys. Rev. B **42**, 1486 (1990).

[25] M. Sieber and K. Richter, Phys. Scr., T **90**, 128 (2001); M. Sieber, J. Phys. A **35**, L613 (2002).

[26] S. Müller, S. Heusler, P. Braun, F. Haake, and A. Altland, e-print nlin.CD/0401021.

[27] O. Bohigas, S. Tomsovic, and D. Ullmo, Phys. Rep. **223**, 43 (1993).

[28] T. A. Brody, J. Flores, J. B. French, P. A. Mello, A. Pandey, and S. S. M. Wong, Rev. Mod. Phys. **53**, 385 (1981).

[29] O. Bohigas, *Mathematical and Computational Methods in Nuclear Physics* (Springer, Berlin, 1984), p. 1.